Aalborg Universitet

Amplitude cancellation influences the association between frequency components in the neural drive to muscle and the rectified EMG signal

Dideriksen, Jakob Lund; Farina, Dario

Amplitude cancellation influences the association between frequency components in the neural drive to muscle and the rectified EMG signal

Jakob Lund Dideriksen[1ʘ], Dario Farina[2ʘ] *

1 Department of Health Science and Technology, Aalborg University, Aalborg, Denmark, **2** Department of Bioengineering, Imperial College London, London, United Kingdom

ʘ These authors contributed equally to this work.
* d.farina@imperial.ac.uk

Abstract

The rectified surface EMG signal is commonly used as an estimator of the neural drive to muscles and therefore to infer sources of synaptic input to motor neurons. Loss of EMG amplitude due to the overlap of motor unit action potentials (amplitude cancellation), however, may distort the spectrum of the rectified EMG and thereby its correlation with the neural drive. In this study, we investigated the impact of amplitude cancelation on this correlation using analytical derivations and a computational model of motor neuron activity, force, and the EMG signal. First, we demonstrated analytically that an ideal rectified EMG signal without amplitude cancellation (EMG_{nc}) is superior to the act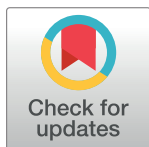ual rectified EMG signal as estimator of the neural drive to muscle. This observation was confirmed by the simulations, as the average coefficient of determination (r^2) between the neural drive in the 1–30 Hz band and EMG_{nc} (0.59±0.08) was matched by the correlation between the rectified EMG and the neural drive only when the level of amplitude cancellation was low (<40%) at low contraction levels (<5% of maximum voluntary contraction force; MVC). This correlation, however, decreased linearly with amplitude cancellation (r = -0.83) to values of r^2 <0.2 at amplitude cancellation levels >60% (contraction levels >15% MVC). Moreover, the simulations showed that a stronger (i.e. more variable) neural drive implied a stronger correlation between the rectified EMG and the neural drive and that amplitude cancellation distorted this correlation mainly for low-frequency components (<5 Hz) of the neural drive. In conclusion, the results indicate that amplitude cancellation distorts the spectrum of the rectified EMG signal. This implies that valid use of the rectified EMG as an estimator of the neural drive requires low contraction levels and/or strong common synaptic input to the motor neurons.

Author summary

The rectified surface EMG signal is commonly used to analyze the neural activation of muscles. However, since this signal is most often exposed to so-called amplitude cancellation (loss of EMG amplitude due to overlap of positive and negative phases of different motor unit action potentials), the frequency content of the rectified EMG may not fully reflect that of the neural drive to the muscle. In this study we prove this notion analytically and demonstrate, using simulations, that the rectified EMG signal accurately reflects the neural drive to the muscle only in a limited set of conditions. Specifically, these conditions include low contraction levels and/or high variability of the neural drive. In other conditions, the rectified EMG signal from a muscle is a poor predictor of its neural input. This finding has potentially large implications for the way neural drive to muscles and neural connectivity (e.g. across muscles or between the brain and a muscle) should be analyzed.

Introduction

The pool of motor neurons innervating a muscle receives a large relative proportion of common synaptic input [1]. The common input is transmitted to the motor neuron output generating the neural drive to the muscle, which is the ensemble of discharge timings of the motor neurons of the pool. The input-output transmission of common input is approximately linear in many conditions [2–4]. Consequently, the analysis of the neural drive to muscles by motor unit recordings has the potential to reveal neural connectivity, e.g. between pools of motor neurons innervating different muscles or between motor neurons and the motor cortex [5,6]. Moreover, the low-frequency components of the neural drive accurately predicts the fluctuations in the isometric force produced by the muscle [7]. Although the neural drive to a muscle can be measured directly from motor unit recordings [8–10], it is more often indirectly inferred from surface electromyographic (EMG) signals.

The amplitude of the EMG signal is associated to the strength of the neural drive. However, it is also influenced by the waveforms of the motor unit action potentials that depend on anatomy and electrode positioning, among other factors [11,12]. The influence of the shape of the action potentials can be partly reduced by standardizing the recording configurations and normalizing the EMG signal. However, the motor unit action potentials also act as high-pass filters of the neural drive (with a cut-off frequency in the range 15–35 Hz) and therefore may reduce the power of low-frequency components of the neural drive [13]. For this reason, rectification of the EMG signal is typically recommended [14,15]. While rectification may recover low frequencies, it introduces distortion in the power spectrum of the EMG signal due to amplitude cancellation [13]. Amplitude cancellation can be defined as the difference in amplitude between the sum of the rectified motor unit action potential trains (no-cancellation condition, which cannot be experimentally measured) and the rectified EMG (that can be actually measured) and can therefore be modeled as a signal-dependent noise term influencing the spectral properties of the rectified EMG [16]. Simulation studies have shown that amplitude cancellation implies a reduction of >50% in the EMG amplitude (i.e., the standard deviation of the EMG or square root of signal power) with respect to the no-cancellation EMG, even at low contraction levels [17,18]. Since the difference between no-cancellation EMG and rectified EMG has a colored spectrum [13], amplitude cancellation may limit the possibility of accurately inferring individual frequency components of the neural drive to muscle from the rectified EMG [13,18]. The degree of this distortion in the

rectified EMG power spectrum is however not yet understood since amplitude cancellation has been previously investigated in terms of its total power but not of the distribution of its power across frequency bands.

Here, we present a theoretical and simulation study that unravels the effect of amplitude cancellation on the frequency components of the rectified EMG. The simulations were based on a realistic computational model that characterized a motor neuron population and the surface EMG and force generated by the muscle it innervates (Fig 1). Two surface EMG signals were simulated. The regular EMG as well as a no-cancellation EMG (EMG$_{nc}$) obtained by rectification of action potentials prior to summation across motor units. Importantly, this implies that EMG$_{nc}$ cannot be measured experimentally, but can only be obtained in simulations. The correlations between the simulated neural drive to the muscle (the ensemble of discharge timings of all motor neurons) and the two simulated EMG signals were quantified to reveal the degree to which this relation was affected by amplitude cancellation. Together, the theoretical and the simulation analyses demonstrate that amplitude cancellation in many conditions disrupts the ability of the rectified surface EMG signal to reflect the neural drive in an accurate way.

Results

Theoretical analysis

We can approximate the rectified EMG (|EMG|) signal as:

$$|EMG(t)| = |s(t) * p(t)| \tag{1}$$

and the no-cancellation EMG (EMG$_{nc}$) as:

$$EMG_{nc}(t) = s(t) * |p(t)|, \tag{2}$$

where t denotes time, $s(t)$ is the neural drive to the muscle, mathematically represented as a series of delta functions centered at the discharge instants of the motor neurons, and $p(t)$ is the average action potential across all motor units. These approximations correspond to assuming that all motor units have the same action potential, as the average waveform among all action potential shapes. The effect of amplitude cancellation can be characterized by the signal $c(t)$, which we define as the difference between the rectified and the no-cancellation EMG:

$$c(t) = EMG_{nc}(t) - |EMG(t)| = s(t) * |p(t)| - |s(t) * p(t)| \tag{3}$$

Amplitude cancellation is the amplitude of the signal $c(t)$.

First, we consider the cross-correlation function ($R(\tau)$) between the no-cancellation EMG and the neural drive to the muscle. This can be derived as follows [19]:

$$\begin{aligned}
R_{EMG_{nc},s}(\tau) &= E\{EMG_{nc}(t) \cdot s(t + \tau)\} \\
&= E\{s(t) * |p(t)| \cdot s(t + \tau)\} \\
&= E\left\{\int_{-\infty}^{\infty} s(\alpha) \cdot |p(t - \alpha)| d\alpha \cdot s(t + \tau)\right\} \\
&= E\left\{\int_{-\infty}^{\infty} s(\alpha) \cdot s(t + \tau) \cdot |p(t - \alpha)| d\alpha\right\} \\
&= \int_{-\infty}^{\infty} R_{ss}(t - \alpha + \tau) \cdot |p(t - \alpha)| d\alpha
\end{aligned} \tag{4}$$
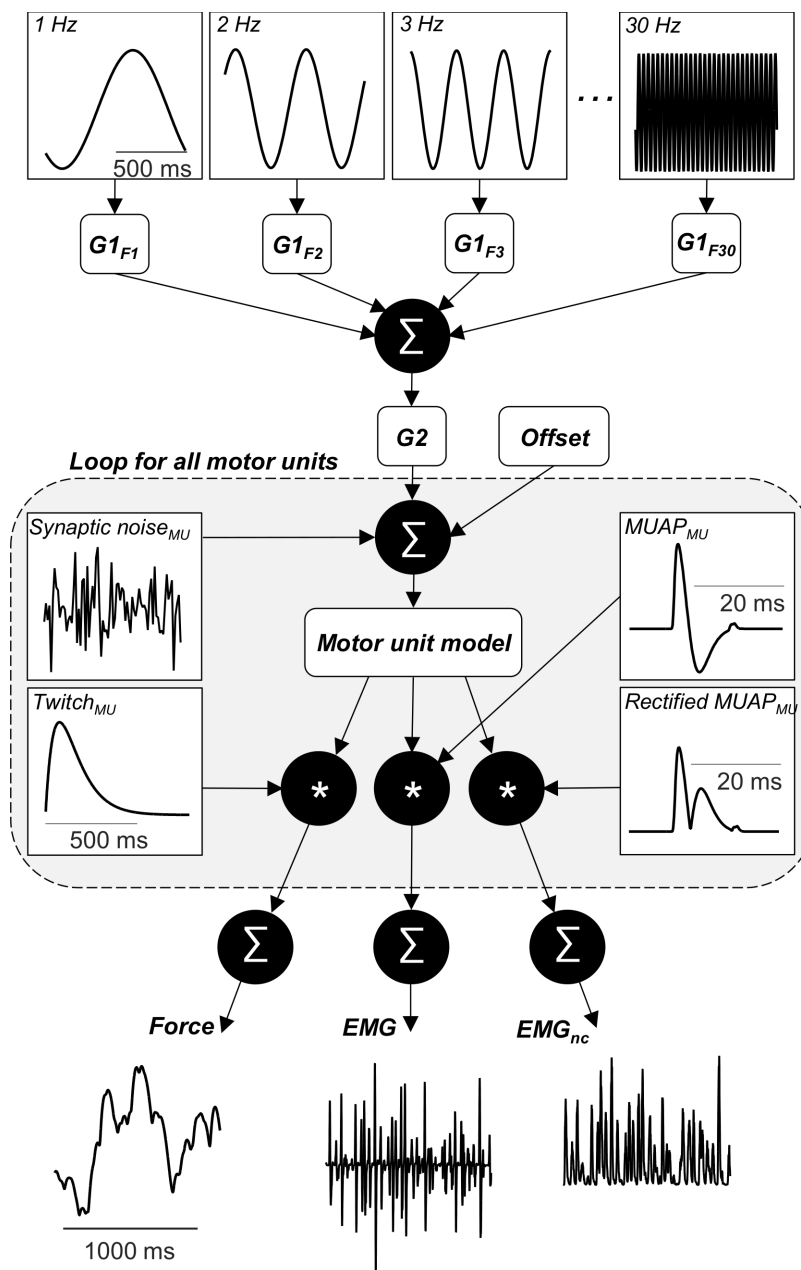
Fig 1. In the model, the common synaptic input to the motor neurons is the sum of 30 sine waves (frequencies: 1–30 Hz), each with an amplitude determined by a gain ($G1_{F1-F30}$) that is determined by the values of a random variable with uniform distribution between 0 and 1. The gain G2 determined the average power of the common input (low, medium, or high) and an offset was added that determined the average contraction level. For each motor unit, independent synaptic noise was added before the motor unit model determined the motor unit spike trains (timing of motor neuron action potentials). For each motor unit, the spike train was convolved with pre-defined templates for the motor unit twitch forces, and the raw and rectified motor unit action potentials. By summation of the force and the EMG signals for each motor unit, the force, EMG, and EMG_{nc} for the full muscle were obtained. The cumulative spike train (CST) was calculated as the algebraic sum of all motor unit spike trains (neural drive to the muscle).

By the substitution $\beta = t-\alpha$, Eq 4 can be re-written as:

$$R_{EMG_{nc},s}(\tau) = \int_{-\infty}^{\infty} R_{ss}(\beta + \tau) \cdot |p(\beta)| d\beta$$
$$= R_{ss}(-\tau) * |p(\tau)|$$
(5)

Since $R_{ss}(\tau)$ is symmetric, Eq 5 can be re-written as:

$$R_{EMG_{nc},s}(\tau) = R_{ss}(\tau) * |p(\tau)|$$
(6)

The cross spectrum (G) between EMG_{nc} and $s(t)$ is the Fourier transform of the cross-correlation function [19]:

$$G_{EMG_{nc},s}(f) = F\{R_{EMG_{nc},s}(\tau)\}$$
$$= F\{R_{ss}(\tau) * |p(\tau)|\}$$
$$= G_{ss}(f) \cdot H_P(f),$$
(7)

where $F\{\cdot\}$ is the Fourier transform operator, $G_{ss}(f)$ is the cross spectrum of the neural drive and $H_p(f)$ is the power spectrum of the rectified action potential. Eq 7 implies that the cross spectrum between EMG_{nc} and $s(t)$ is equivalent to G_{ss} only if $H_p(f) = 1$ for all f. In this case, the coherence between the no-cancellation EMG and the neural drive to muscle (cross-spectrum normalized by auto-spectra) would be equal to 1 for all frequencies. This is the case only if the rectified action potential is a delta function, thus not altering the neural drive. Therefore, a perfect correlation between EMG_{nc} and the neural drive never occurs. Instead, the level of correlation depends on the spectrum of the action potential.

Next, we consider the correlation between the rectified EMG and the neural drive. This is derived as follows:

$$R_{|EMG|,s}(\tau) = E\{|EMG(t)| \cdot s(t + \tau)\}$$
$$= E\{|s(t) * p(t)| \cdot s(t + \tau)\}$$
$$= E\{|\int_{-\infty}^{\infty} p(\alpha) \cdot s(t-\alpha)d\alpha| \cdot s(t + \tau)\}$$
(8)

Since $s(t) \geq 0$ for all t, Eq 8 can be re-written as:

$$R_{|EMG|,s}(\tau) = E\{|\int_{-\infty}^{\infty} p(\alpha) \cdot s(t-\alpha) \cdot s(t + \tau)d\alpha|\}$$
$$\leq E\{\int_{-\infty}^{\infty} |p(\alpha)| \cdot s(t-\alpha) \cdot s(t + \tau)d\alpha\}$$
$$= \int_{-\infty}^{\infty} |p(\alpha)| \cdot R_{ss}(\tau+\alpha)d\alpha$$
(9)

Comparing Eqs 5 and 9, we get:

$$R_{|EMG|,s}(\tau) \leq R_{EMG_{nc},s}(\tau), \forall \tau$$
(10)

Eq 10 shows that the correlation between the rectified EMG and the neural drive is always equal to or smaller than the correlation between the no-cancellation EMG and the neural drive. The two correlation levels will the same only if the action potential waveform is only positive, which would correspond to the absence of cancellation. Therefore, although the no-cancellation EMG is not a perfect estimate of the neural drive, it would provide better estimates of the neural drive to muscle than the rectified EMG. The difference between the

rectified EMG and the no-cancellation EMG is the cancellation signal term ([Eq 3](#)) and cancellation determines the decrease in association between the corresponding EMG signal and the neural drive. The above derivations show that in all conditions, cancellation is detrimental to the association between EMG and the neural drive to muscle.

Simulations

Using the computational model ([Fig 1](#)), the activity of the motor neuron population, the force, and the EMG ("regular" rectified EMG and EMG$_{nc}$) were simulated. Based on a synaptic input signal, the cumulative spike train (CST; algebraic sum of all motor unit spike trains) representing the neural drive to the muscle [2,7], the muscle force, the rectified and the no-cancellation EMG signals were simulated. The no-cancellation EMG was obtained by summing the rectified motor unit action potentials. EMG$_{nc}$, which cannot be experimentally derived, was used to assess the effect of amplitude cancellation on the rectified EMG when inferring frequency components of the neural drive to muscle [17]. The synaptic input to each motor neuron consisted of a signal common to all motor units and an independent noise source [2]. The common synaptic input was modeled as the sum of a series of 30 sine waves (frequency: 1, 2, 3, . . . 30 Hz) with random phases and amplitudes and with an offset. Across the simulations, we varied the number of motor units and the characteristics of the common input. Each combination of these settings was repeated 15 times. The amplitude of each imposed sine wave was assigned a random value in each repetition. Using linear regression analysis, the strength of the association between the power of the neural drive and each of the EMG signals (rectified EMG and EMG$_{nc}$) at each imposed frequency was obtained across all simulated conditions.

The number of recruited motor units and their average discharge rate increased with the offset of the common input. Across all simulations with the low offset (contraction level: 1.4% MVC) and low common input variability, 18% of the motor units were recruited with an average discharge rate of 5.9 pulses per second (pps). The number of recruited units and their discharge rates increased steadily as the offset increased, reaching 53% recruited motor units, on average discharging at 27.7 pps at the highest offset (contraction level: 17.1% MVC). The discharge rates across the motor unit pool were highest for the smallest motor units. An increase in the variability of the common synaptic input also determined an increase in the number of recruited motor units and their discharge rates. On average, the number of recruited motor units increased by 22 percentage points and the average discharge rate by 3.7 pps when increasing the variability of synaptic input in the analyzed range. The impact of these different recruitment patterns on the evoked force is illustrated in [Fig 2](#). As expected, the main determinant of force variability was the amplitude of the variability of the common input to the motor neuron population. In addition, the force was less variable when simulated with a larger motor neuron population, as previously shown [20]. In the simulations with low amplitude of common input, the standard deviation of force was 0.3–0.5% of MVC, which corresponds to the variability experimentally observed when young healthy subjects are asked to maintain a steady contraction level with visual feedback [21–24]. For example, the coefficient of variation (standard deviation divided by the mean) of force is usually >5% for low contraction levels (<5% MVC) and stabilizes at <3% at higher contraction levels [21–24], which is similar to the values for low common input in [Fig 2(D)](#). Conversely, force fluctuations are expected to be substantially greater during most functional tasks, such as gait, where force modulation is needed. In this way, the simulations with higher variability of the common input ([Fig 2B and 2C](#)) represents such conditions in a more accurate way.

[Fig 3](#) shows the neural drive to the muscle (CST), the EMG signals and the force in the time and frequency domain in one simulation. The median frequency of the raw EMG signal over
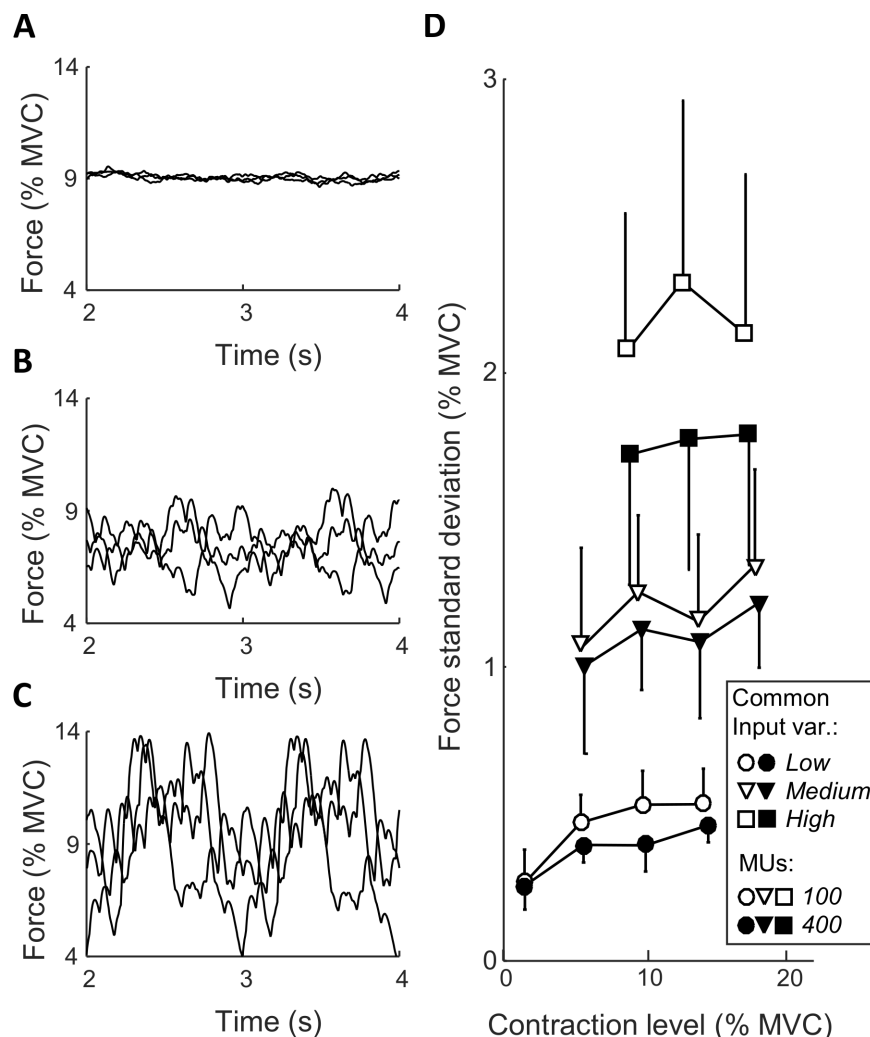
Fig 2. Three representative examples of simulated forces with low (A), medium (B), and high (C) amplitudes of the variability of the common synaptic input to a population of 400 motor neurons. Panel D illustrates the force standard deviation (mean±std) for all simulated conditions. Here, the symbols along each line represent different offsets of the common synaptic input and the different lines represent different amplitudes of common input variability and/or different number of motor units.

all simulations with low common input variability was 72.0±14.8 Hz, which is within the range of experimentally observed values [25–27]. This figure enables a visual comparison between the characteristics of the signals, and the degree to which the neural drive is reflected in the other signals. The variation in the power of the neural drive across the different frequencies reflects the random amplitudes of the sine waves composing the common synaptic input [2]. In the time-domain, the amplitude of EMG_{nc} was always greater than for the rectified EMG indicating the effect of amplitude cancellation (Fig 3C). The two EMG signals, however, were relatively similar and usually exhibited peaks at the same time instants. Consequently, their spectral characteristics were similar, but not identical (Fig 3D). The power spectrum of the EMG_{nc} closely resembled that of the neural drive (Fig 3(B)), to a greater extent than for the rectified EMG. This illustrates the distortion imposed by amplitude cancellation in the frequency domain. As expected, the low-pass filtering properties of the motor unit twitches
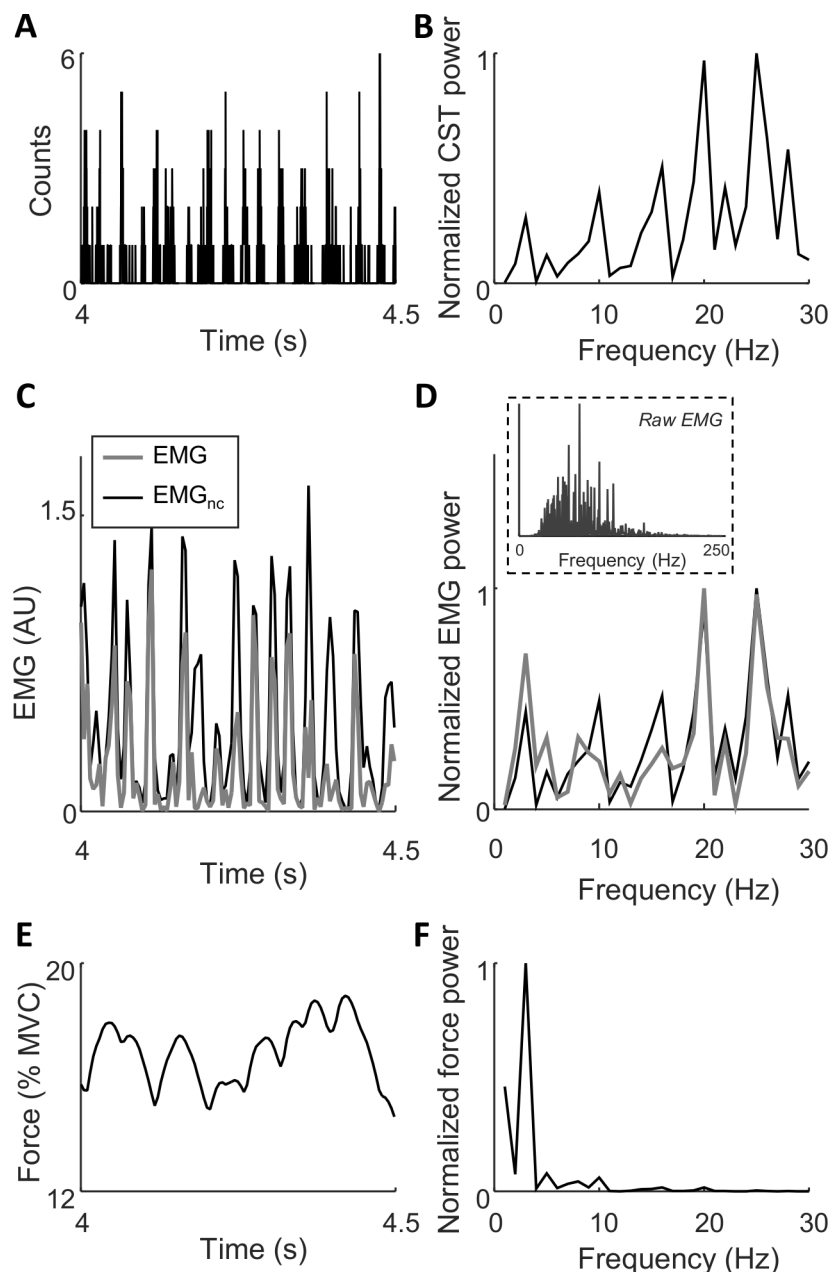
Fig 3. Temporal and spectral representation of the cumulative spike train (CST; A, B), the rectified EMG and EMGnc (C, D), and force (E, F). In panel D, the normalized power spectrum of the raw (unrectified) EMG signal in the 0–250 Hz range is included in the dashed box. In this example, the muscle consisted of 100 motor units, the amplitude of the variability of the common synaptic input was high (force standard deviation: 1.8%MVC), and the average contraction level was 14.9%MVC. The power spectra (B, D, F) indicate power only for integer frequencies that were the frequency components used to simulate the common input.

implied that only the lowest frequency components of the neural drive were transmitted to force (Fig 3F).

Fig 4 shows examples of the linear relation between the distribution of power across frequencies for the CST and for the two EMG signals across 15 repetitions. Specifically, the power at 2, 15, and 28 Hz are shown for simulations with high common input amplitude. For the
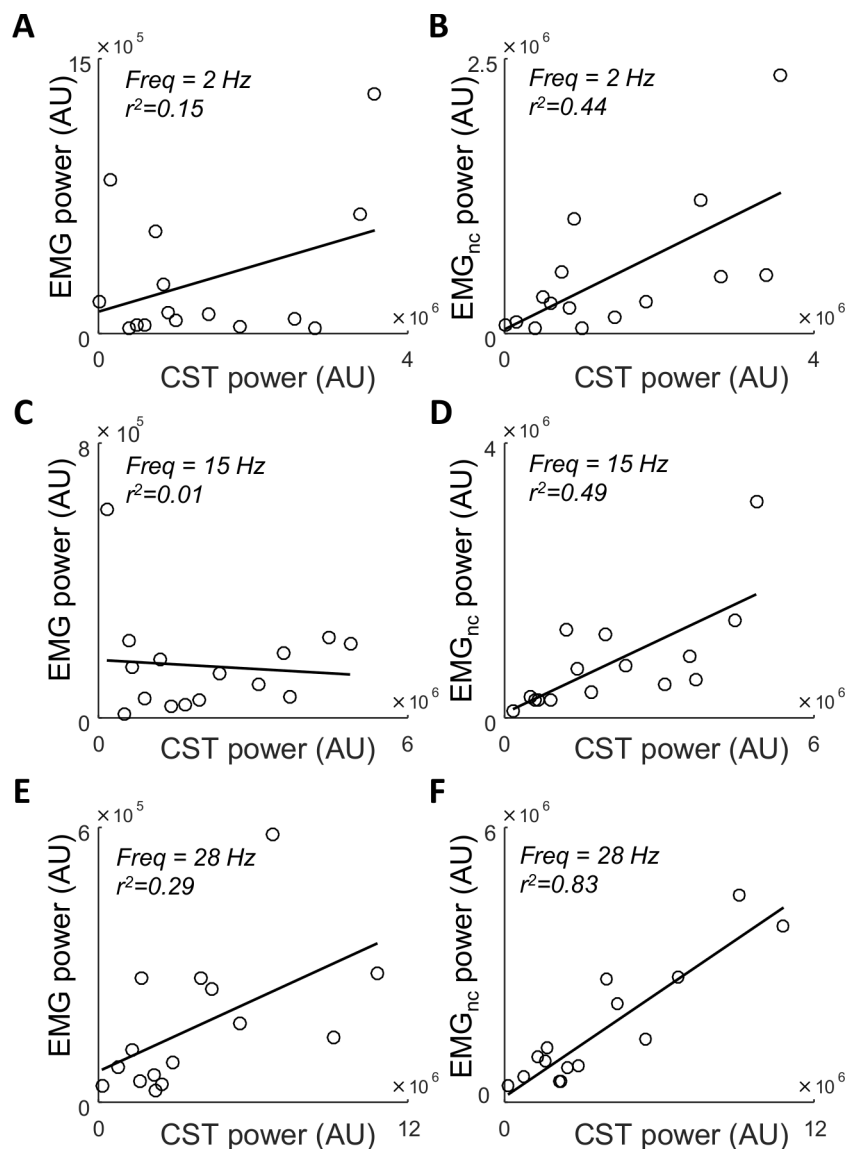
Fig 4. Linear relations between the power at three frequencies (2 Hz: A, B. 15 Hz: C, D. 28 Hz: E, F) in the CST and the rectified EMG (A, C, F) as well as the CST and EMG$_{nc}$ (B, D, F). The data in these examples represent simulations in which the muscle consisted of 100 motor units, the amplitude of the variability of the common synaptic input was high (force standard deviation: 1.8%MVC), and the average contraction level was 14.9%MVC. In each panel, each circle represents the power of the two signals in one of the 15 simulations conducted with these parameter values.

https://doi.org/10.1371/journal.pcbi.1006985.g004

EMG$_{nc}$, an association was present for these three frequencies ($r^2 \geq 0.44$), whereas the association was much weaker for the rectified EMG. For the rectified EMG, however, the linear correlation was strongest at the highest frequencies ($r^2 = 0.15$ at 2 Hz, Fig 4(A); $r^2 = 0.29$ at 28 Hz, Fig 4(E)). These observations are confirmed by average values of coefficient of determination across all simulations (Fig 5). Here, average r^2 is represented as a function of contraction level for different frequency bands across the simulation conditions. Across all conditions, the correlation between EMG$_{nc}$ and CST was high (mean $r^2 = 0.59 \pm 0.08$) and was largely unaffected by contraction level. Conversely, the correlation between EMG and CST was relatively high at low contraction levels ($r^2 \geq 0.37$), and decreased greatly when the contraction level (and thus

Fig 5. Values of r² for the linear relations between CST and rectified EMG and EMGₙc respectively, as functions of the contraction levels across all simulations. In each panel, black lines represent the relation between CST and rectified EMG (symbols represent average values for the 1–5 Hz, 6–15 Hz, and 16–30 Hz frequency bands, respectively; see inset in panel C), while grey lines represent the relation between CST and EMGₙc (each line represents the same frequency bands as for CST-EMG). Panels A, B, C s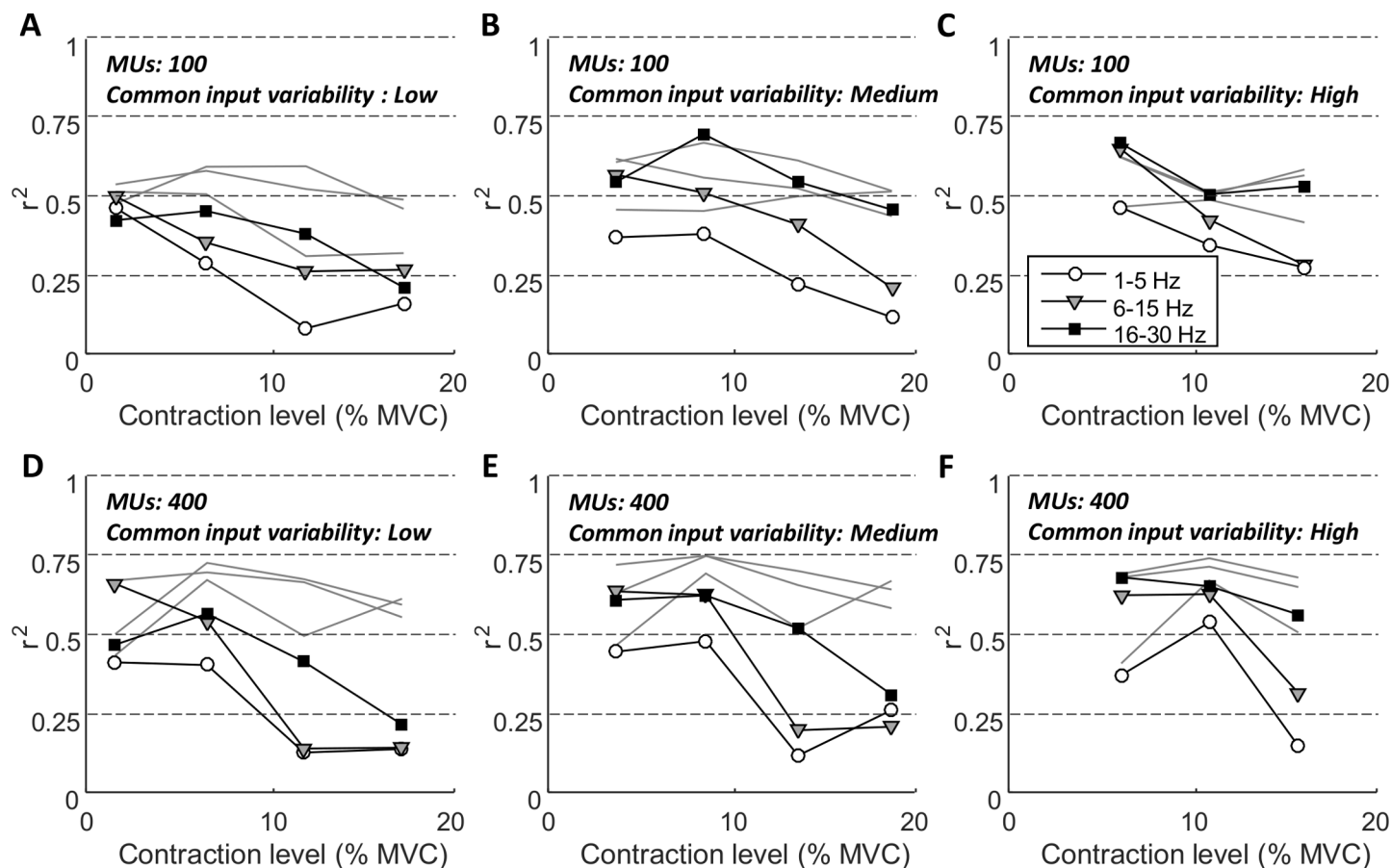how results for simulations with 100 motor units, while panels D, E, F represent 400 motor units. Panels A, D represent low variability of the common synaptic input to the motor neurons, panels B, E medium variability, and panels C, F high variability.

amplitude cancellation) increased. This trend was observed across all conditions, but the decrease was strongest when the amplitude of the common input was low. For example, r² was 0.19±0.05 with low common input and 0.35±0.16 with high common input, for contraction levels >10% MVC. The lowest correlations were typically observed for the lowest frequencies. For example, at contraction levels between 5–10% MVC, r² for the beta band (16–30 Hz) was on average 0.32±0.14 higher than for the delta band (1–5 Hz). Finally, the number of motor units did not have a large effect on the values of r².

The values of amplitude cancellations across all simulations were between 37 and 71%, which corresponded to the ranges reported in previous simulation studies [17,18]. In general, the lowest levels of amplitude cancellation were achieved with low contraction levels and high common input. The level of amplitude cancellation was strongly negatively correlated with the average correlation between CST and rectified EMG across all imposed frequencies (r = -0.83; Fig 6). While the values of r² were similar to those of EMGₙc (≥0.5) at low levels of amplitude cancellation (<40%), these values decreased at higher levels of amplitude cancellation. Conversely, in the simulations where the correlation between the rectified EMG and CST was low (i.e., those with high levels of amplitude cancellation) the correlation between EMGₙc and CST was unaffected.
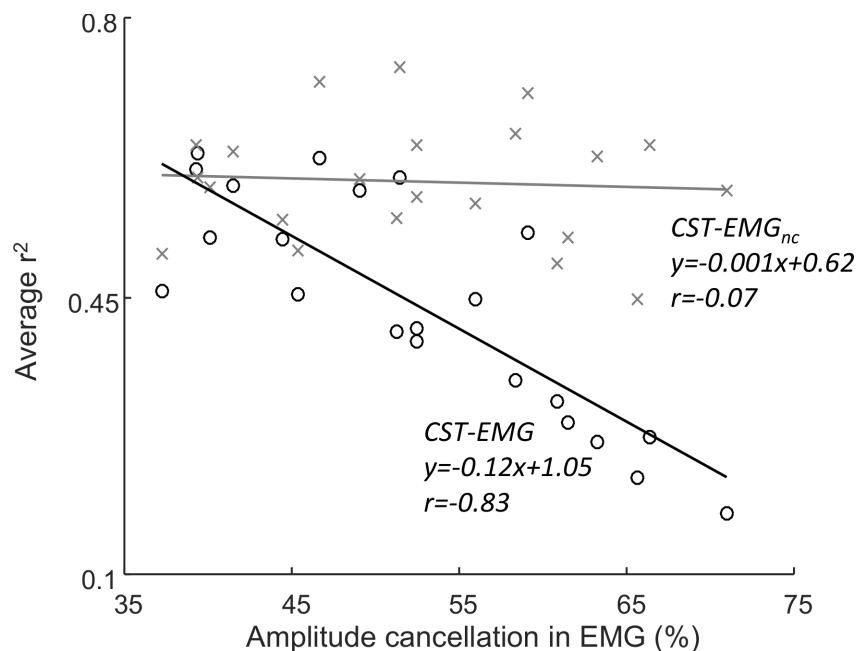
Fig 6. The relation between the average r^2 (across all frequencies) for CST-EMG and the degree of amplitude cancellation in the EMG (black circles) across all simulation conditions. In addition, the average r^2 for CST-EMG$_{nc}$ (grey x's) is included. Here, the value on the axis represents the level of amplitude cancellation from the EMG in the same simulation.

Discussion

In this study, we systematically investigated the relation between the magnitude of amplitude cancellation in the rectified surface EMG signal and the ability of this signal to reflect the neural drive to the muscle. The neural drive is the ensemble of discharge timings of all motor neurons innervating the muscle. We imposed common synaptic input to the motor neurons in the frequency band 1–30 Hz and therefore analyzed the neural drive in this frequency range. First, using an analytical approach we demonstrated that amplitude cancellation implies that the rectified EMG is not an optimal estimator of the neural drive. Next, the simulation results indicated that amplitude cancellation strongly impairs this ability to a degree where some frequency components of the neural drive would only be weakly present in the EMG (Fig 6). As also shown in previous studies, the level of amplitude cancellation was low when few motor units were active, but increased when more motor units were recruited [17,18]. This trend was clearly reflected in the simulations, where the correlation between the frequency components in the neural drive and in the rectified EMG was high at low contraction levels, but decreased rapidly when the contraction level increased (Fig 5). An important finding of the study was that the rate of this decrease depended on the strength and frequency band of the neural drive component. Specifically, this implies that strong oscillating components in the neural drive are required to overcome the distortion arising due to amplitude cancellation. Moreover, the result suggests that low-frequency components of the neural drive in the rectified EMG are more susceptible to this distortion. Finally, the simulations confirmed the observation from the derivations (Eq 7) that even without amplitude cancellation, the EMG signal does not provide a perfect characterization of the neural drive (average r^2 for EMG$_{nc}$ and CST was 0.59), because of the effect of the shape of the action potentials.

These finding can explain a number of previous experimental observations. For example, although the neural drive during steady isometric contractions often contains strong low-frequency components (<5 Hz) [1], these are typically not observed in coherence analyses involving the rectified EMG [28–31]. Conversely, in dynamic tasks such as gait, where strong low-frequency components of the neural drives determine substantial force fluctuations [7], high levels of EMG-EMG coherence (indicating strong shared neural drive between two EMG signals) can be observed in the delta band [32–36]. Similarly, when subjects are asked to generate a steadily increasing isometric force from rest to maximum (i.e., the strongest low-frequency variation in the neural drive that can be generated), the EMG amplitude typically displays an increasing trend similar to that of force [37–39]. Together, these observations indicate that low-frequency components of the neural drive can be detected by the rectified EMG, but only if their power is sufficiently high. Furthermore, whereas low-frequency components of the neural drive appear to be disrupted in the rectified EMG during steady contractions, neural inputs to motor neurons at higher frequency bands (>20 Hz) have been observed in such conditions from EMG analysis [15,28–31], which supports the finding that EMG amplitude cancellation primarily distorts the low frequencies.

Overall, the results identify a limitation related to the analysis of the neural drive to muscles based on the EMG signal. This limitation has implications for many methods for investigating the neural control of movement. Such applications include muscle synergy analysis that investigates modular control of activation of multiple muscles [40,41]. In such analysis, the rectified EMG signals are usually low-passed filtered—sometimes with cut-off frequencies as low as 4 Hz [42]—which implies a risk that the signals considered (only the lowest frequencies) are heavily corrupted due to amplitude cancellation. This may particularly be the case when applied to conditions with little muscle force variability such as postural control [43,44], whereas applications such as gait [45] likely involves sufficiently large variations in the low-frequency content of the neural drive to minimize the distortion of the EMG spectrum. Similarly, the results also have implications for the comparison between the rectified EMG and mechanical measures (force/acceleration), which have been used, e.g., to explain the role of neural oscillations in physiological tremor [46]. It should be underlined, however, that this study does not suggest that all analyses of rectified EMG signals are invalid. Conversely, the results imply that the rectified EMG is often exposed to some degree of distortion due to amplitude cancellation, which may affect study outcomes to varying degrees depending on the characteristics of the motor task.

Since amplitude cancellation reflects the amount of overlap of motor unit action potentials, its magnitude can be reduced by increasing the selectivity of the recording and/or recording derivation. The most selective interface is intramuscular EMG, where recordings with almost no overlap between action potentials can be achieved at low contraction levels [47]. Although the amplitude cancellation, and thus the distortion of the EMG signal, is minimal in such recordings, the high selectivity may imply a poor representation of the neural drive from a global analysis of the signal properties. Depending on the contraction characteristics, the activity of a critical number of motor units needs to be reflected in the signal for it to accurately represent the neural drive [2]. In this way, increasing the recording selectivity as a solution to this problem implies a trade-off between reducing amplitude cancellation and maintaining a sufficient number of motor units contributing to the signal. It is, however, unknown, what characterizes the optimal trade-off between these factors and if a precise characterization of the neural drive can be achieved, even in the optimal case. Instead, a more plausible solution to the problem could be to base the analysis on motor unit spike trains rather than on EMG [2]. Although the process of spike train identification adds an additional level of complexity to experimental protocols, recent advances in EMG decomposition enable non-invasive identification of large numbers of spike trains [8–10].

In the theoretical analysis, the EMG signals were analytically described on the basis on one action potential waveform (Eqs 1 and 2). This is a simplification with respect to experimental conditions where action potentials across a motor unit pool exhibit variations in amplitude as well as duration [48]. Whereas such variations will affect the filtering properties of the action potentials (Eq 7), they will not impact on the main conclusion drawn from the theoretical analysis. Indeed, the theoretical predictions have been fully confirmed by the numerical simulation results, that were achieved using realistic action potentials for each individual motor unit.

The primary limitation of the model is that the simulated discharge rate of the motor units does not saturate above a critical excitation limit. Experimentally, this is observed when discharge rates of motor units recruited at low forces cease to increase with increasing force, while the discharge rate of motor units recruited at higher forces continue to increase [49]. Conversely, in the model, the discharge rates of all motor units (once recruited) increase monotonically with input excitation level. The rate at which motor unit discharges saturate varies substantially across muscles [50], but the simulated discharge rates for the smallest motor units at the highest contraction levels (approximately 30 pps) are above the rates that would normally be assumed as their maximum [24]. In spite of the fact that the discharge rates of low-threshold motor units at some point cease to increase, evidence suggests that their discharge rates continue to reflect variation in the common synaptic input [51]. To the best of our knowledge, no computational motor neuron model accurately captures this behavior. Instead, we selected the model with the most realistic amplitude and phase response [52] and limited the simulations to relatively low contraction levels where discharge rates of low-threshold motor units did not greatly exceed those observed experimentally. Nevertheless, the failure of the model to fully recreate realistic conditions may have biased the results. When the simulated discharge rates of low-threshold motor units exceeded the rate required for tetanic force (approximately 20–24 pps [53]), an increase in the offset of the synaptic input would imply not only recruitment of new motor units (serving to increase the contraction level) but also additional action potentials discharged by low-threshold units (not generating more force). Thereby, the density of action potentials, and thus the level of amplitude cancellation, would be higher than in experimental conditions for that particular contraction level. This would imply that the simulations to some degree overestimated the rate by which the correlation between the rectified EMG and the CST declined with contraction level (Fig 5). However, we believe that the impact of this error on the outcome of the study is relatively small. Indeed, first, in most simulation conditions the correlation already began to decline at approximately 12% MVC where simulated discharge rates presumably corresponded to natural conditions (Fig 5). Second, the additional action potentials at the highest simulated contraction levels are those with the lowest amplitude due to the relatively low innervation numbers of low-threshold motor units. Therefore, their potential impact on the EMG signal is minimal.

Finally, a limitation of the simulation strategy is that, the average amplitude of the sine waves imposed as common synaptic input to all motor neurons across the 15 repetitions was uniform for all frequencies. This assumption may not apply to experimental conditions. Since synaptic inputs at different frequency bands are often attributed to specific neural structures [51,54,55], some frequency-dependent variability in the amplitude would be expected across tasks. For example, synaptic input at approximately 8 Hz has been attributed to stretch-sensitive afferent feedback [56], whose synaptic strength can be modulated by presynaptic inhibition in task-dependent ways [57]. In addition, the strength of the synaptic input in the beta band also depends on the motor task [58]. This implies that the relation between the variability of the neural drive and the muscle force (Fig 2) cannot be generalized to all conditions. For example, it is possible that a contraction with low variability of synaptic input at low frequencies (i.e. little force variability) has a strong beta band input. In this case, the force steadiness

cannot be used as a measure for the potential distortion of the spectral components of the rectified EMG at high frequencies. However, the linearity of the motor neuron pool [2–4] implies that the components of the neural drive reflecting synaptic input from different neural structures can be identified more accurately from the CST than from EMG.

In conclusion, the study demonstrates that amplitude cancellation impairs the degree to which the rectified EMG signal reflects the neural drive to the muscle, except in conditions with low contraction levels and/or highly variable common synaptic input. This distortion of the EMG signal affects primarily its lowest frequency components.

Methods

Computational model

The model architecture is illustrated in Fig 1. To summarize, the synaptic input to the pool of motor neurons determined their discharge pattern. Based on those patterns, the force, EMG, and EMG$_{nc}$ were simulated.

Motor neuron model

The number of motor neurons was set to 100 or 400. Each motor neuron was simulated with Hodgkin Huxley-type models [59,60] and consisted of two compartments (soma and dendrite) for motor neurons with six conductances (leak conductances for the soma and dendrite, compartment coupling conductances between the 2 compartments, and 3 voltage-dependent conductances, sodium Na, fast potassium Kf, and slow potassium Ks) and four state variables (m, h, n, q). Membrane-specific capacitance was set to µ1 F and axial resistivity to 70 Ωcm. The soma-specific resistance ranged from 1.15 to 0.65 kΩcm^2 and the dendrite-specific resistance from 14.4 to 6.05 kΩcm^2. Equilibrium potentials were 120 mV for sodium and 10 mV for potassium, while the equilibrium potential of the membrane and leakage voltages were 0 mV. Input to the motor neurons was simulated as injected currents into the soma compartment. The ranges of model parameters were adopted from a previous study [61] with exponential distributions across the motor neuron population (i.e. many low-threshold motor units, few high-threshold motor units) [53]. The differential equations of the model were solved in MATLAB 2015a with the function "ode15s."

The simulated motor neuron spike trains were used as inputs to simulate EMG and force. In addition, the algebraic sum of all motor unit spike trains (CST) was obtained as a representation of the neural drive to the muscle.

EMG model

A library of motor unit action potentials was simulated using a previously proposed model [62]. The model included 101,276 individual muscle fibers (average length: 100 mm) with innervation zones distributed in a 10 mm region around half of the fiber length. The muscle fibers were located in a cylindrical shape (thickness: 27.5 mm; conductivity: 0.1 S/m in radial and transverse directions, 0.5 S/m in longitudinal direction) around a bone (radius: 7.5 mm; conductivity: 0.02 S/m). In addition, a subcutaneous layer (thickness: 1 mm; conductivity: 0.05 S/m) and skin (thickness: 2 mm; conductivity: 1 S/m) surrounded the muscle. For the simulations, 15 electrode pairs (circular; radius: 2 mm; inter-electrode distance: 10 mm) were included equally distributed around this cylinder halfway between the innervation zone and the end of the fibers. For each electrode, 100 or 400 motor units were selected within a circular area (radius: 7 mm or 14 mm, respectively) centered 5.3 or 10.5 mm below each electrode. For each motor unit pool, the innervation numbers were exponentially distributed (range: 6–69).

In this way, 15 different sets of motor unit action potentials were generated for each of the two muscles consisting of 100 or 400 motor units. Interference EMG signals were simulated as the sum of the motor unit action potential trains (convolution of the motor neuron spike trains with the action potentials assigned to that motor neuron). In addition to the interference EMG signal, a EMG_{nc} was simulated by rectifying the action potentials prior to convolution with the spike trains.

Force model

Muscle force was simulated based on the motor unit spike trains using a previously proposed model [53]. According to this model, the motor unit twitches were modelled as critically damped second-order system where the peak amplitude varied 100-fold across the motor unit population. The contraction time (time from twitch onset to peak) ranged from 30 to 90 ms. Both twitch parameters were distributed according to an exponential relation, so there were most low-amplitude, slow-twitch units. In addition, the gain of each twitch depended in a non-linear way on the instantaneous motor unit discharge rate.

The MVC force was estimated in pilot simulations as the force elicited by the muscle when all motor units were active at a discharge rate equivalent to the peak discharge rate proposed in previous simulation studies [53].

Simulation strategy

The synaptic input to each motor neuron consisted of a common and an independent term and an offset. The independent term was low-passed filtered (<100 Hz) white Gaussian noise scaled in order to get a realistic variability of the inter-spike intervals (coefficient of variation: 10–30% [22,63,64]) in the absence of common input. The common synaptic input was the sum of 30 sine waves (frequency: 1–30 Hz) with random phases. This range of frequencies were selected as they represent those most often analyzed in experimental conditions. The gains $G1_{F1-F30}$ (Fig 1) were random values selected from a uniform distribution between 0 and 1. The gain G2 determined the average variability of the common input and was scaled to get different values of the strength of the common input and of the variability of force. Across simulations, three different values were assigned to G2: $5.7 \cdot 10^{-5}$, $1.5 \cdot 10^{-4}$, $2.4 \cdot 10^{-4}$. These values ensured standard deviations of force equivalent to those observed when subjects aim to maintain stable force with visual feedback and equivalent to more functional, force-varying tasks, respectively (see *Results*). The offset was scaled to simulate different average contraction levels and was assigned the values $3.5 \cdot 10^{-3}$, $3.8 \cdot 10^{-3}$, $4.0 \cdot 10^{-3}$, $4.3 \cdot 10^{-3}$. These values ensured average contraction levels between 1 and 20% MVC. All combinations of these values for G2 and offset were simulated using motor neuron populations consisting of 100 and 400 motor units, respectively. The combination with the highest G2 ($2.4 \cdot 10^{-4}$) and the highest offset ($4.3 \cdot 10^{-3}$) was excluded since it evoked contraction levels >20% MVC and thereby involved unrealistic motor unit discharge patterns (see *Discussion* for details). In total, this implied 22 simulated conditions. Each condition was repeated 15 times. In each of these repetitions, the independent synaptic noise, the phase of each sine wave, and the values assigned to $G1_{F1-F30}$ varied. Furthermore, the EMG signals for each of these repetitions were based on different sets of motor unit action potentials (see *EMG model* for details).

Analysis

Across the 15 repetition of each simulation condition the amplitude of each of the 30 imposed frequencies (1–30 Hz) were extracted from the power spectra of the CST and the two EMG signals (rectified EMG and EMG_{nc}). The linear correlations between these power amplitudes of

the CST and the rectified EMG, and the CST and EMG_{nc} were analyzed separately for each frequency. For each simulation condition, the average values for r^2 in the 1–5 Hz band (delta band), the 6–15 Hz band (alpha band), and the 16–30 Hz band (beta band) were calculated. In this way, the association between the neural drive and the EMG was identified across input frequencies. For each condition, the level of amplitude cancellation was calculated as the ratio between the average values of the cancellation term (Eq 3) and EMG_{nc}.

Author Contributions

Conceptualization: Jakob Lund Dideriksen, Dario Farina.

Data curation: Jakob Lund Dideriksen, Dario Farina.

Formal analysis: Jakob Lund Dideriksen, Dario Farina.

Investigation: Jakob Lund Dideriksen, Dario Farina.

Methodology: Jakob Lund Dideriksen, Dario Farina.

Validation: Jakob Lund Dideriksen, Dario Farina.

Writing – original draft: Jakob Lund Dideriksen, Dario Farina.

Writing – review & editing: Jakob Lund Dideriksen, Dario Farina.

References

1. Negro F, Yavuz UŞ, Farina D. The human motor neuron pools receive a dominant slow-varying common synaptic input. J Physiol. 2016; 594: 5491–5505. https://doi.org/10.1113/JP271748 PMID: 27151459

2. Farina D, Negro F, Dideriksen JL. The effective neural drive to muscles is the common synaptic input to motor neurons. J Physiol. 2014; 49: 1–37.

3. Negro F, Farina D. Linear transmission of cortical oscillations to the neural drive to muscles is mediated by common projections to populations of motoneurons in humans. J Physiol. 2011; 589: 629–637. https://doi.org/10.1113/jphysiol.2010.202473 PMID: 21135042

4. Stegeman DF, van de Ven WJM, van Elswijk G a., Oostenveld R, Kleine BU. The α-motoneuron pool as transmitter of rhythmicities in cortical motor drive. Clin Neurophysiol. 2010; 121: 1633–1642. https://doi.org/10.1016/j.clinph.2010.03.052 PMID: 20434397

5. Gallego J, Dideriksen J, Holobar A, Ibanez J, Pons J, Louis E, et al. Influence of common synaptic input to motor neurons on the neural drive to muscle in essential tremor. J Neurophysiol. 2015;113.

6. Laine CM, Martinez-valdes E, Falla D, Mayer F, Farina D. Motor Neuron Pools of Synergistic Thigh Muscles Share Most of Their Synaptic Input. J Neurosci. 2015; 35: 12207–12216. https://doi.org/10.1523/JNEUROSCI.0240-15.2015 PMID: 26338331

7. Negro F, Holobar A, Farina D. Fluctuations in isometric muscle force can be described by one linear projection of low-frequency components of motor unit discharge rates. J Physiol. 2009; 587: 5925–38. https://doi.org/10.1113/jphysiol.2009.178509 PMID: 19840996

8. Negro F, Muceli S, Castronovo AM, Holobar A, Farina D. Multi-channel intramuscular and surface EMG decomposition by convolutive blind source separation. J Neural Eng. 2016;13.

9. Muceli S, Poppendieck W, Negro F, Yoshida K, Hoffmann KP, Butler JE, et al. Accurate and representative decoding of the neural drive to muscles in humans with multi-channel intramuscular thin-film electrodes. J Physiol. 2015; 593: 3789–3804. https://doi.org/10.1113/JP270902 PMID: 26174910

10. Marateb HR, McGill KC, Holobar A, Lateva ZC, Mansourian M, Merletti R. Accuracy assessment of CKC high-density surface EMG decomposition in biceps femoris muscle. J Neural Eng. 2011; 8: 66002.

11. Dimitrova NA, Dimitrov G V., Nikitin OA. Neither high-pass filtering nor mathematical differentiation of the EMG signals can considerably reduce cross-talk. J Electromyogr Kinesiol. 2002; 12: 235–246. PMID: 12121680

12. Lindström LH, Magnusson RI. Interpretation of Myoelectric Power Spectra: A Model and Its Applications. Proc IEEE. 1977; 65: 653–662.

13. Negro F, Keenan K, Farina D. Power spectrum of the rectified EMG: when and why is rectification beneficial for identifying neural connectivity? J Neural Eng. 2015; 12: 36008.

14. Halliday D, Farmer S. On the need for rectification of surface EMG. J Neurophysiol. 2010; 3547. https://doi.org/10.1152/jn.00222.2010 PMID: 20530508

15. Ward NJ, Farmer SF, Berthouze L, Halliday DM. Rectification of EMG in low force contractions improves detection of motor unit coherence in the beta-frequency band. J Neurophysiol. 2013; 110: 1744–50. https://doi.org/10.1152/jn.00296.2013 PMID: 23904490

16. Day SJ, Hulliger M. Experimental simulation of cat electromyogram: Evidence for algebraic summation of motor-unit action-potential trains. J Neurophysiol. 2001; 86: 2144–2158. https://doi.org/10.1152/jn.2001.86.5.2144 PMID: 11698507

17. Keenan KG, Farina D, Maluf KS, Merletti R, Enoka RM. Influence of amplitude cancellation on the simulated surface electromyogram. J Appl Physiol. 2005; 98: 120–131. https://doi.org/10.1152/japplphysiol.00894.2004 PMID: 15377649

18. Farina D, Negro F, Jiang N. Identification of common synaptic inputs to motor neurons from the rectified electromyogram. J Physiol. 2013; 591: 2403–18. https://doi.org/10.1113/jphysiol.2012.246082 PMID: 23507877

19. Papoulis A, Pillai SU. Probability, Random Variables and Stochastic Processes. 4th ed. McGraw-Hill Europe; 2002.

20. Dideriksen JL, Negro F, Enoka RM, Farina D. Motor unit recruitment strategies and muscle properties determine the influence of synaptic noise on force steadiness. J Neurophysiol. 2012; 107: 3357–3369. https://doi.org/10.1152/jn.00938.2011 PMID: 22423000

21. Sosnoff JJ, Valantine AD, Newell KM. Independence between the amount and structure of variability at low force levels. Neurosci Lett. 2006; 392: 165–169. https://doi.org/10.1016/j.neulet.2005.09.010 PMID: 16188384

22. Moritz CT, Barry BK, Pascoe MA, Enoka RM. Discharge rate variability influences the variation in force fluctuations across the working range of a hand muscle. J Neurophysiol. 2005; 93: 2449–2459. https://doi.org/10.1152/jn.01122.2004 PMID: 15615827

23. Brown RE, Edwards DL, Jakobi JM. Sex differences in force steadiness in three positions of the forearm. Eur J Appl Physiol. 2010; 110: 1251–1257. https://doi.org/10.1007/s00421-010-1600-x PMID: 20737167

24. Barry BK, Pascoe MA, Jesunathadas M, Enoka RM. Rate coding is compressed but variability is unaltered for motor units in a hand muscle of old adults. J Neurophysiol. 2007; 97: 3206–3218. https://doi.org/10.1152/jn.01280.2006 PMID: 17360826

25. Kienbacher T, Habenicht R, Starek C, Mair P, Wolf M, Paul B, et al. The potential use of spectral electromyographic fatigue as a screening and outcome monitoring tool of sarcopenic back muscle alterations. J Neuroeng Rehabil. 2014;11.

26. Allison GT, Fujiwara T. The relationship between EMG median frequency and low frequency band amplitude changes at different levels of muscle capacity. Clin Biomech. 2002; 17: 464–469.

27. Hermens HJ, Bruggen TAM v, Baten CTM, Rutten WLC, Boom HBK. The median frequency of the surface EMG power spectrum in relation to motor unit firing and action potential properties. J Electromyogr Kinesiol. 1992; 2: 15–25. https://doi.org/10.1016/1050-6411(92)90004-3 PMID: 20870523

28. Baker SN, Kilner JM, Pinches EM, Lemon RN. The role of synchrony and oscillations in the motor output. Exp Brain Res. 1999; 128: 109–117. PMID: 10473748

29. Kilner JM, Baker SN, Salenius S, Jousmäki V, Hari R, Lemon RN. Task-dependent modulation of 15–30 Hz coherence between rectified EMGs from human hand and forearm muscles. J Physiol. 1999; 516: 559–570. https://doi.org/10.1111/j.1469-7793.1999.0559v.x PMID: 10087353

30. Hansen S, Hansen NL, Christensen LOD, Petersen NT, Nielsen JB. Coupling of antagonistic ankle muscles during co-contraction in humans. Exp Brain Res. 2002; 146: 282–292. https://doi.org/10.1007/s00221-002-1152-3 PMID: 12232685

31. Dideriksen JL, Negro F, Falla D, Kristensen SR, Mrachacz-Kersting N, Farina D. Coherence of the surface EMG and common synaptic input to motor neurons.

32. Jaiser S, Baker M, Baker S. Intermuscular coherence in normal adults: Variability and changes with age. PLoS One. 2016; 11: e0149029. https://doi.org/10.1371/journal.pone.0149029 PMID: 26901129

33. Fisher KM, Zaaimi B, Williams TL, Baker SN, Baker MR. Beta-band intermuscular coherence: A novel biomarker of upper motor neuron dysfunction in motor neuron disease. Brain. 2012; 135: 2849–2864. https://doi.org/10.1093/brain/aws150 PMID: 22734124

34. Moon H, Kim C, Kwon M, Chen YT, Onushko T, Lodha N, et al. Force control is related to low-frequency oscillations in force and surface EMG. PLoS One. 2014; 9: e109202. https://doi.org/10.1371/journal.pone.0109202 PMID: 25372038

35. Norton JA, Gorassini M. Changes in Cortically Related Intermuscular Coherence Accompanying Improvements in Locomotor Skills in Incomplete Spinal Cord Injury. J Neurophysiol. 2005; 95: 2580–2589.

36. Van Asseldonk EHF, Campfens SF, Verwer SJF, Van Putten MJAM, Stegeman DF. Reliability and agreement of intramuscular coherence in tibialis anterior muscle. PLoS One. 2014;9.

37. Lawrence JH, De Luca CJ. Myoelectric signal versus force relationship in different human muscles. J Appl Physiol. 1983; 54: 1653–1659. https://doi.org/10.1152/jappl.1983.54.6.1653 PMID: 6874489

38. Maluf KS, Shinohara M, Stephenson JL, Enoka RM. Muscle activation and time to task failure differ with load type and contraction intensity for a human hand muscle. Exp Brain Res. 2005; 167: 165–177. https://doi.org/10.1007/s00221-005-0017-y PMID: 16044306

39. Inman VT, Ralston HJ, Saunders JB, Feinstein B, Wright EW. Relation of human electromyogram to muscular tension. Electroencephalogr Clin Neurophysiol. 1952; 4: 187–194. PMID: 13033796

40. Ting LH, McKay JL. Neuromechanics of muscle synergies for posture and movement. Current Opinion in Neurobiology. 2007. pp. 622–628. https://doi.org/10.1016/j.conb.2008.01.002 PMID: 18304801

41. d'Avella A, Saltiel P, Bizzi E. Combinations of muscle synergies in the construction of a natural motor behavior. Nat Neurosci. 2003; 6: 300–308. https://doi.org/10.1038/nn1010 PMID: 12563264

42. Clark DJ, Ting LH, Zajac FE, Neptune RR, Kautz SA. Merging of Healthy Motor Modules Predicts Reduced Locomotor Performance and Muscle Coordination Complexity Post-Stroke. J Neurophysiol. 2010; 103: 844–857. https://doi.org/10.1152/jn.00825.2009 PMID: 20007501

43. McKay JL, Ting LH. Functional muscle synergies constrain force production during postural tasks. J Biomech. 2008; 41: 299–306. https://doi.org/10.1016/j.jbiomech.2007.09.012 PMID: 17980370

44. Ting LH. A Limited Set of Muscle Synergies for Force Control During a Postural Task. J Neurophysiol. 2004; 93: 609–613. https://doi.org/10.1152/jn.00681.2004 PMID: 15342720

45. Martino G, Ivanenko YP, D'Avella A, Serrao M, Ranavolo A, Draicchio F, et al. Neuromuscular adjustments of gait associated with unstable conditions. J Neurophysiol. 2015; 114: 2867–82. https://doi.org/10.1152/jn.00029.2015 PMID: 26378199

46. Vernooij CA, Reynolds RF, Lakie M. A dominant role for mechanical resonance in physiological finger tremor revealed by selective minimization of voluntary drive and movement. J Neurophysiol. 2013; 109: 2317–2326. https://doi.org/10.1152/jn.00926.2012 PMID: 23407354

47. McGill KC, Lateva ZC, Marateb HR. EMGLAB: An interactive EMG decomposition program. J Neurosci Methods. 2005; 149: 121–133. https://doi.org/10.1016/j.jneumeth.2005.05.015 PMID: 16026846

48. Farina D, Negro F, Gazzoni M, Enoka RM. Detecting the Unique Representation of Motor-Unit Action Potentials in the Surface Electromyogram. J Neurophysiol. 2008; 100: 1223–1233. https://doi.org/10.1152/jn.90219.2008 PMID: 18497352

49. Fuglevand AJ, Lester RA, Johns RK. Distinguishing intrinsic from extrinsic factors underlying firing rate saturation in human motor units. J Neurophysiol. 2015; 113: 1310–1322. https://doi.org/10.1152/jn.00777.2014 PMID: 25475356

50. Enoka RM, Fuglevand AJ. Motor unit physiology: some unresolved issues. Muscle Nerve. 2001; 24: 4–17. PMID: 11150961

51. De Luca CJ, LeFever RS, McCue MP, Xenakis AP. Control scheme governing concurrently active human motor units during voluntary contractions. J Physiol. 1982; 329: 129–142. PMID: 7143247

52. Goroso DG, Cisi RRL, Kohn AF. The amplitude and phase responses of the firing rates of some motoneuron models. BioSystems. 2000; 58: 33–39. PMID: 11164628

53. Fuglevand AJ, Winter DA, Patla AE. Models of recruitment and rate coding organization in motor-unit pools. J Neurophysiol. 1993; 70: 2470–2488. https://doi.org/10.1152/jn.1993.70.6.2470 PMID: 8120594

54. Vallbo AB, Wessberg J. Organization of motor output in slow finger movements in man. J Physiol. 1993; 469: 673–691. PMID: 8271223

55. Brown P, Salenius S, Rothwell JC, Hari R. Cortical correlate of the piper rhythm in humans. J Neurophysiol. 1998; 80: 2911–2917. https://doi.org/10.1152/jn.1998.80.6.2911 PMID: 9862895

56. Erimaki S, Christakos C. Coherent motor unit rhythms in the 6–10 Hz range during time-varying voluntary muscle contractions: neural mechanism and relation to rhythmical motor control. J Neurophysiol. 2008; 99: 473–83. https://doi.org/10.1152/jn.00341.2007 PMID: 18057114

57. Baudry S, Enoka RM. Influence of load type on presynaptic modulation of Ia afferent input onto two synergist muscles. Exp Brain Res. 2009; 199: 83–88. https://doi.org/10.1007/s00221-009-1951-x PMID: 19639306

58. Laine CM, Valero-Cuevas FJ. Intermuscular Coherence Reflects Functional Coordination. J Neurophysiol. 2017; 118: 1775–1783. https://doi.org/10.1152/jn.00204.2017 PMID: 28659460

59. Negro F, Farina D. Factors Influencing the Estimates of Correlation between Motor Unit Activities in Humans. PLoS One. 2012;7.

60. Dideriksen J, Negro F, Farina D. The optimal neural strategy for a stable motor task requires a compromise between the level of muscle co-contraction and synaptic gain of afferent feedback. J Neurophysiol. 2015; 114: 1895–911. https://doi.org/10.1152/jn.00247.2015 PMID: 26203102

61. Cisi RR, Kohn AF. Simulation system of spinal cord motor nuclei and associated nerves and muscles, in a Web-based architecture. J Comput Neurosci. 2008; 25: 520–542. https://doi.org/10.1007/s10827-008-0092-8 PMID: 18506610

62. Farina D, Mesin L, Martina S, Merletti R. A Surface EMG Generation Model with Multilayer Cylindrical Description of the Volume Conductor. IEEE Trans Biomed Eng. 2004; 51: 415–426. https://doi.org/10.1109/TBME.2003.820998 PMID: 15000373

63. Clamann HP. Statistical analysis of motor unit firing patterns in a human skeletal muscle. Biophys J. 1969; 9: 1233–1251. https://doi.org/10.1016/S0006-3495(69)86448-9 PMID: 5824412

64. Matthews PB. Relationship of firing intervals of human motor units to the trajectory of post-spike after-hyperpolarization and synaptic noise. J Physiol. 1996; 492: 597–628. PMID: 9019553